Gyre formation in open and deep lacustrine embayments: The example of Lake Geneva, Switzerland

A.M. Razmi [a*,1], U. Lemmin [a], D. Bouffard [b], A. Wüest [b,c], R.E. Uittenbogaard [d], D.A. Barry [a]

[a] Laboratoire de technologie écologique (ECOL), Institut d'ingénierie de l'environnement, Faculté de l'environnement naturel, architectural et construit (ENAC), Ecole polytechnique fédérale de Lausanne (EPFL), CH-1015 Lausanne, Switzerland. Emails: ulrich.lemmin@epfl.ch, andrew.barry@epfl.ch, amir.razmi@epfl.ch

[b] Physics of Aquatic Systems Laboratory – Margaretha Kamprad Chair, Institut d'ingénierie de l'environnement, Faculté de l'environnement naturel, architectural et construit (ENAC), Ecole polytechnique fédérale de Lausanne (EPFL), Lausanne, Switzerland. Emails: damien.bouffard@epfl.ch, alfred.wueest@epfl.ch

[c] Eawag, Swiss Federal Institute of Aquatic Science and Technology, Kastanienbaum, Switzerland. Email: alfred.wueest@eawag.ch

[d] Deltares, Rotterdamseweg 185 2629 HD Delft, The Netherlands. Email: rob.uittenbogaard@deltares.nl

[*] Author to whom all correspondence should be addressed Ph. +1 (617) 335-7391, fax. +1 (617) 258-8850.

[1] Present address: Environmental Fluid Mechanics Laboratory, Parsons Laboratory for Environmental Science, Department of Civil and Environmental Engineering, Massachusetts Institute of Technology (MIT), Cambridge, Massachusetts, USA.

Abstract

Numerical simulations were carried out to investigate gyres within open lacustrine embayments subjected to parallel-to-shore currents. In such embayments, gyre formation occurs due to flow separation at the embayment's upstream edge. High momentum fluid from the mixing layer between the embayment and offshore flows into the embayment and produces recirculating flow. Systematic numerical experiments using different synthetic embayment configurations were used to examine the impact of embayment geometry. Geometries included embayments with different aspect ratios, depths and embayment corner angles. The magnitudes of the recirculation and turbulent kinetic energy (TKE) in the embayment vary significantly for angles in the range 40° to 55°. Embayments with corner angles less than 50° have much stronger recirculation and TKE, other parameters remaining the same. The numerical findings are consistent with gyre formation observed in two embayments located in Lake Geneva, Switzerland, and thus help explain flow patterns recorded in lacustrine shoreline regions.

Keywords: Hydrodynamics; Open embayment; Flow separation; Turbulence; Gyre; Corner angle, Non-stratified flow

1 Introduction

Lake nearshore regions are of great importance, since they provide freshwater for drinking-water supplies, recreational activities, industrial heating and cooling systems, etc. In addition, these regions often have significant ecological value (macrophytes, reed stands, spawning grounds for fish). At the same time, the quality of these waters may be severely affected when pollutants from sewage outfall, agricultural contaminants and storm drain discharge enter the near-shore region [1]. Clearly, the fate of such contaminants depends on near-shore flow dynamics, particularly within embayments. Gyre formation in embayments, for example, can entrap lake water for lengthy periods, which in turn may result in degraded water quality and pollutant accumulation in nearshore sediments [2].

We consider here flow within open embayments, which constitute a less often studied class of embayments. In coastal morphology, a shoreline indentation is considered an open embayment if it provokes a nearshore circulation pattern [3]. Generally, the flow of a fluid past a cavity will create shear-induced circulation – consisting of one or more gyres – within it [4, 5]. There is a comprehensive literature on flow structures within different cavity geometries [6]. Shankar and Deshpande [5] and Erturk [7] provided reviews on cavity flow structures. Investigations of cavities and their impacts on flow in river channels were reported also [8-10]. Several studies considered gyre formation within semi-enclosed embayments, i.e., where the embayment is, in part, separated from the open water by a land boundary [11]. Key results of relevant studies are summarized in §2.1.

Apart from steady longshore flows, gyres can form in open oceanic embayments due to wave or tidally driven flows, as was considered by Signell et al. [12]. Elwell [13] revealed that embayment gyres can procedure when a tidal stream is separated at the upstream embayment boundary. For open embayments under oceanic tidal flows, geometry, tide period and offshore flow velocity were found to be the key factors determining gyre formation [13]. These results are not directly valid for open lacustrine embayments where tides are negligible and in which winds are the main force driving the currents [14].

Recent measurements and 3D modelling of an open lacustrine embayment (Vidy Bay) on the north shore of a large lake (Lake Geneva; Fig. 1) revealed that a gyre can form under certain

wind conditions [15]. Two main flow patterns in the embayment can occur: one with a gyre and another one in which currents flow mainly parallel-to-shore. A slight modification in the mean wind angle can markedly change the circulation in the main basin of Lake Geneva (Grand Lac, Fig. 1), which affects pelagic currents in front of Vidy bay. The combination of current direction and upstream embayment geometry may cause current separation and a gyre to form within the embayment. Gyre formation was found not to depend on thermal stratification, internal waves, embayment water depth or spatial variability of the wind field [15].

This paper examines the formation of gyres within open lacustrine embayments having different embayment geometries. The results obtained by systematically varying relevant forcing and embayment geometry allow for a quantitative analysis of conditions that affect gyre formation and their magnitude in open embayments. Field measurements from two embayments on Lake Geneva (Switzerland) were used to evaluate the applicability of the numerical simulation results.

2 Background and methods

2.1 Flow structure of open embayments

Flow past a single open cavity is characterized by the formation of a shear (or mixing) layer at the cavity mouth and a recirculation zone inside it [16, 17]. The velocity gradient at the leading (upstream) edge of the cavity forms vortical structures that are advected downstream and impinge on the trailing (downstream) edge of the cavity [17]. The vorticity patches become entrained and are advected along the cavity mouth. This separated shear layer in front of the cavity creates a recirculation zone within the cavity [4]. The gyre that develops in the embayment mainly has a 2D nature, which can be simulated either by depth-averaged numerical models that use a constant eddy viscosity coefficient [9], or depth-averaged k-ε turbulence models [18].

In the literature there are many studies on 2D shear-layer entrainment showing that the precise nature of cavity flows is highly dependent on geometry and flow parameters including the free stream velocity and turbulence level [19, 20]. Caton et al. [21] suggested that the source of 2D turbulence structures is the gradient of stream velocity near the upstream (leading) cavity edge. These structures create a shear layer that can separate the flow in the cavity from the main

stream, and thus affect the mass exchange across it. Further downstream, the 2D structures become unstable and collapse into 3D turbulence in deep waters [22]. In shallow-water flows, bed friction drains energy from 2D turbulence motions. It contributes to energy cascades and a reduction of the mixing layer growth rate. In the present study, gyre formation in very shallow embayments, i.e., where bottom friction affects gyre formation, is not considered.

Below we describe two analyses. First, simulations are performed on a synthetic embayment covering a wide range of conditions. The results can then be used to analyze flow patterns in embayments in natural settings. Second, the results of these synthetic simulations are validated using simulations from Lake Geneva.

2.2 Gyre formation in synthetic embayments

Delft3D-FLOW is a widely used hydrodynamic modelling package [23]. The model solves the Reynolds-Averaged Navier-Stokes equations using the *k*-ε turbulence closure for an incompressible fluid with the Boussinesq approximation and hydrostatic-pressure assumption. The governing equations are discretized using finite-differences. In the horizontal direction, curvilinear numerical cells with orthogonal boundaries were used. In the vertical direction σ co-ordinates were applied. Chezy's roughness formula [23] was applied at the bottom boundary.

The model here was used to simulate flow in typical synthetic embayments controlled by a parallel-to-shore offshore current (Fig. 2). Bed slope has a minor effect on gyre formation in deep embayments, although it can influence the location of the gyre [15]. Simulations were carried out in a uniform-depth, synthetic embayment in which the geometry was systematically varied, as was the offshore current magnitude. The imposed flow and embayment geometry determine the exchange of mass, momentum, and energy between the embayment and the main basin. Exchange takes place across the shear layer in front of the embayment and is affected by the gyre dynamics inside the embayment.

Figure 2 displays the setup used. It consists of an embayment of length *L*, width *W*, and corner angle α at the embayment's upstream and downstream ends. The main gyre circulation (Γ) magnitude was calculated using $\Gamma = \oint V_s ds$, where V_s is the tangential velocity along a closed path (*S*, with differential element *s*) bounding the region of vorticity [25]. The integration path was

based on the largest closed streamline in the flow, as shown by the oval in Fig. 2. The depth-averaged velocity was used to determine the circulation magnitude within the embayment and depends on offshore velocity (U), the mean turbulent kinetic energy (TKE, k), and the corner angle (α). The embayment aspect ratio is defined as length-to-width ratio, $Ar = L/W$.

Flow dynamics in open embayments depend on the Reynolds number, Re. Previous studies [13] took the length scale in the Re definition as the length L of open embayment (Fig. 2), because of the significant exchange across the shear layer interface. However, the longitudinal gyre size, l (Fig. 2), within the embayment is more relevant to energy dissipation, and hence we take $Re = Ul/\boldsymbol{\nu}$, where $\boldsymbol{\nu}$ is the kinematic viscosity and U is the speed of the parallel-to-shore current (Fig. 2). We consider the length of the recirculation region after the leading edge of the embayment (l) in the direction of the major axis along the shoreline (i.e., reattachment distance from the leading edge) as the characteristic length in calculating Re and scaling the circulation magnitude in our study. L appears in the geometrical factor Ar, and is also varied in the simulations.

Energy input into the modelled embayment occurs only through the external longshore current and we therefore scale the TKE with U^2. Similarly, we scale the circulation magnitude as Γ/Ul. This quantity characterizes the efficiency of the transfer of the external flow momentum to the recirculation.

We performed a set of numerical experiments to explore the dependence of the circulation on a range of offshore current speeds (U = 0.1, 1, 5, 10 cm s^{-1}), embayment aspect ratios (Ar = 2, 3, 4, 6, 8, obtained using different embayment lengths with W = 1 km), and corner angles ($\alpha = 0°$ to 60°). In addition, various (uniform) embayment depths are considered. Table 1 summarizes the numerical experiments performed in this study. For all cases, the model was run until a quasi-steady state was reached.

2.3 Delft3D-FLOW modelling of Lake Geneva

Delft3D-FLOW was used previously to simulate the hydrodynamics of Lake Geneva [15, 16]. In the vertical direction, σ coordinates were applied with 40 non-equidistant levels for the real-time numerical model [26]. The vertical discretization was refined near the water surface with a resolution of 0.5% of the local water depth. Since the lake was modelled as being initially

quiescent, the simulations commenced with a hydrodynamic spin-up. Details of the real-time lake and Vidy Bay hydrodynamic model set-up and calibration were given by Razmi et al. [15, 26], who validated the hydrodynamic model using data from 2005, 2010 and 2011. The model's predictions agreed with an accompanying Lagrangian drifter experiment that captured local current patterns. Likewise, Delft3D-FLOW numerical results were found to compare reasonably well with ADCP (Acoustic Doppler Current Profiler) and temperature profiles measured in Vidy Bay. For the simulations reported here, unstructured triangular grids were generated using the flexible mesh option in Delft3D [24], which allowed handling of the sharp boundaries employed for the synthetic embayment geometries. Convergence tests ensured that the results were grid-independent in the horizontal plane.

2.4 Study area for the real embayment and definition of cases

Figure 1 shows Lake Geneva and the location of Vidy Bay and Morges Bay on its north shore. As seen in Fig. 1, although the landward recesses in the coastline in both embayments are not marked, they are classified as open lacustrine embayments since their coastline geometry may induce nearshore gyres [3]. They are used as examples to evaluate the impact of morphology and local flow characteristics on nearshore gyres. Vidy Bay and Morges Bay are also of environmental interest since their water quality is subject to local stress. Vidy Bay, for example, receives treated effluent from a large wastewater treatment plant (WTP). As shown in Fig. 1, the WTP outfall is located within Vidy Bay at ~500 m offshore (E534.670, N151.540, Swiss coordinates [27]) and at ~30 m depth [28].

Circulation in Vidy Bay and Morges Bay was investigated in two field measurement campaigns. The first was based on Eulerian measurements with ADCPs while the second followed a Lagrangian approach using drifters.

- ADCP measurements

Two ADCPs were deployed in Vidy Bay during Jan and Feb 2012. One ADCP was located close to the embayment shoreline, ~0.5 km offshore (E534.672, N151.520, Swiss coordinates; A1 in Fig. 1). Profiles of currents were measured over the depth range 3 - 30 m (2-m interval) with a 2.5-min temporal resolution. Another ADCP was positioned ~1.5 km offshore (E534.050,

N150.600, Swiss coordinates; A2 in Fig. 2). In this case, current profiles were measured over the depth range 6 - 130 m (4-m interval) on a 5-min increment.

- Drifter measurements

Drifters were released near the outfall in Vidy Bay on 9 Aug 2011. Table 2 reports the wind conditions before the drifter release. The drifters were composed of a float with an on-board GPS and a drogue attached to a cable. The drifters followed the currents in the upper layer between 2 - 5 m depth. The experimental campaign and its instrumentation were described by Razmi et al. [15].

3 Results and discussion

3.1 Synthetic embayments

We first present results from the simulation of synthetic embayments, with cavity-like shapes.

- Effect of varying the embayment morphology

An extensive series of simulations was performed. We consider first some representative results, i.e., corner angles $\alpha = 0°$ and $40°$ for $Ar = 3$. Modelled mean flow structure, vorticity and TKE fields are displayed in Fig. 3. The variation of normalized circulation with the corner angle and aspect ratio is shown in Fig. 4 for representative cases, $Ar = 3$, 4, 6, and 8 and various corner angles (0° - 60°).

As is apparent in Figs. 3b and e, vortical structures develop due to the relatively large horizontal gradient of the currents and momentum at the embayment's leading edge. The vorticity patches are advected downstream and impinge on the trailing edge of the embayment forming a shear layer in front of the embayment. The shear layer located at the embayment mouth separates the offshore flow from the embayment, in which a recirculation zone forms (Figs. 3a, d). The distribution of low and high vorticity patches is in good agreement with previous numerical modelling and experimental results of flow past lateral rectangular embayments [4].

At the embayment upstream edge, stream flow velocity is substantially reduced in the shoreward direction. This large velocity gradient causes a vertical depth-averaged structure and 2D

turbulence, which in turn leads to the formation of a shear layer at the mouth of the embayment starting from the upstream corner. This shear layer separates the water inside and outside the embayment. Momentum from the shear layer is transferred toward the internal boundaries of the embayment giving rise to smaller scale eddies.

The 2D-resolved TKE fields follow a similar trend for the various cases considered. A representative case of lacustrine embayments is presented in Fig. 3f where the vorticity patches generated in front of the embayment mouth are advected downstream into the vicinity of the trailing edge. This results in relatively higher TKE levels in the downstream embayment regions. Overall, we can conclude that the TKE attenuates from downstream towards the upstream embayment region (Fig. 3f). The distribution of TKE is also consistent with previous numerical results on flow past rectangular cavities [6]. Compared to the flow for the embayment with $\alpha = 0°$, the magnitude of the vorticity at the leading edge reduces as the corner angle increases from $\alpha = 0°$ to 40° (e.g., maximum value of the vorticity field for $\alpha = 0°$ and 40° reduces from 2.2×10^{-4} to 1.8×10^{-4} s^{-1}).

The variation of normalized circulation with α and *Ar* is shown in Fig. 4. For all cases, Γ attenuates with increasing α. Steep gradients are observed in the curves between angles $\alpha = 40°$ and 55°. In contrast, this variation is not pronounced in the range between $\alpha = 0°$ and 40°. In agreement with previous studies on cavity flow [29, 30], there is a possibility of an eddy when a sudden variation of the cross section occurs in the flow. For a corner angle near $\alpha = 55°$, the circulation is very low.

For $Ar = 8$ or higher, the flow resembles a backward facing step in the upstream cavity and a forward facing step in the downstream cavity region with no interaction between these flows [31]. In this case, the shear layer sweeps inside the embayment, reattaches to the external current again, and a recirculation region forms in the upstream region of the embayment, forming a flow similar to that over a backward facing step [32].

For $Ar = 2$ to 6, the shear layer bridges the embayment opening and reattaches only near the trailing edge. By contrast, at large aspect ratios (e.g., $Ar = 8$), a drop of the circulation magnitude occurs. These results are consistent with previous experimental work on the flow over a cavity,

where it was found that separated flow can reattach at the trailing edge in rectangular cavities with $Ar < 6$ [32].

Non-dimensional values of TKE versus the corner angle are presented in Fig. 4b. The mean value of TKE over an embayment area was calculated and found to be attenuated with increasing α. This occurs since the momentum gradient decreases in the shear layer at the leading edge. As with the circulation variation, this reduction of normalized TKE is more pronounced from α = 40° to α = 55°. Similarly, the normalized TKE is maximal for α = 0° at the given aspect ratio due to the large velocity gradient at the leading edge of the embayment.

The effect of bathymetry on the gyre formation was also investigated. Uniform bathymetry was compared with variable embayment depth from 10 to 80 m. Figure 5 shows the variation of the normalized circulation with uniform topography (uniform depth of 10, 40, 80 m). In contrast to the pronounced variations observed in the circulation related to the geometry of the embayment, no evident changes were seen as the embayment depth varied.

- Effect of varying the external current speed

We considered embayments with $Ar = 2$ and 4 and α = 0° and 40° under different offshore velocities (Fig. 6). The data for these four geometries showed the same basic trend: growth of circulation with increasing offshore current speed. Higher *Re* increases momentum exchange and vorticity entrainment, leading to higher vorticity fields and circulation magnitude within the embayment. The non-dimensional circulation magnitude reaches its peak at $U = 1$ cm s^{-1} due to increased production of TKE in the shear layer. Simultaneously, The TKE production causes more energy dissipation in the flow field, and thus leads to slower growth of the non-dimensional Γ as *Re* increases in the cases with $U > 1$ cm s^{-1}.

3.2 Real embayments – Vidy Bay and Morges Bay

- ADCP observations and numerical modelling

Time- and depth-averaged ADCP velocity measurements over the duration of an event are presented in Fig. 7. Observations between 15 and 16 Jan 2012 (Table 2), during which there was a north-easterly wind (locally known as Bise) at an angle of 17° (all wind angles are degrees

azimuth), indicate that there was an eastward current direction close to the shore and westward offshore. In contrast, the ADCP measurements for 3-5 Feb 2012 (Bise at an angle of 40°) showed a similar flow direction (westward) in both the nearshore and offshore of Vidy Bay. Based on previous findings on Vidy Bay current patterns [15], for winds at an angle of less than 25°, a gyre can be generated in the embayment, whereas longshore currents are dominant for larger angle Bise winds. Numerical modelling was conducted to simulate the circulation patterns in the embayment for wind angles 17° and 40°. Likewise, we calculated depth-averaged velocity vectors during each event (Fig. 7). Both the simulation and measurements indicate a gyre in the embayment 15-16 Jan 2012. Modelled current velocity vectors for 3-5 Feb 2012, however, show no gyre in Vidy Bay.

- Drifter observations and numerical modelling

A drifter was released near the WTP outfall location in Vidy Bay (Fig. 1, from 8 Aug 2011, 12:00 AM to 9 Aug 2011, 7:00 AM) and moved towards the west of the embayment, eventually entering Morges Bay. A Bise (average direction of 27° based on Pully observations, Table 2) wind field was measured before and during the deployment. Currents were simulated during this period (Fig. 8). The drifter trajectory is consistent with current patterns simulated numerically. The numerical trajectory was determined from particle tracking results in the topmost model layer. The measured and computed tracks of the released drifters indicate that currents followed a parallel-to-shore direction in Vidy Bay, whereas currents formed a clockwise gyre within Morges Bay (Fig. 8).

3.3 Prediction of real embayment behavior from numerical modelling results

In §2.3 we examined flow characteristics for synthetic embayments with different shoreline morphologies. Those results are now compared to the current patterns measured in Vidy Bay and Morges Bay. For Vidy Bay, the upstream corner angle (α) is about 50° and its aspect ratio is between 3 and 4. For Morges Bay, the upstream corner angle is about 40° and the aspect ratio is less than 3. Compared to Vidy Bay, the smaller corner angle for Morges Bay generates greater turbulence from the leading edge, which increases the likelihood of gyre formation within the embayment for a given offshore current velocity (Fig. 4a, b). As shown in §3.2, a longshore current was observed in Vidy Bay whereas there was gyre formation in Morges Bay. It is also

predicted that the circulation pattern in Vidy has a greater variability (in terms of gyre presence/absence) than in Morges Bay for a given longshore current, since Vidy Bay's corner angle is close to the critical angle ($\alpha = 60°$) in which gyre formation in the embayment is possible. Therefore, small variations of the pelagic current direction at the leading edge of Vidy Bay can switch the flow within the embayment from a recirculating gyre to a longshore current. Such small variations in the pelagic currents are induced by changes in the large gyre pattern within the Grand Lac of Lake Geneva [33]. By contrast, Morges Bay has a smaller corner angle, which engenders less variability of circulation patterns within the embayment, because there is a lower possibility of switching from longshore flow to embayment gyres.

4 Conclusions

Numerical results show that the flow patterns in open lacustrine embayments are mainly parallel-to-shore or in the form of a gyre. The type of pattern formed depends on the angle between the longshore (i.e., outside the embayment) current and the leading edge of the embayment. The impact of α (upstream embayment angle), Ar (embayment aspect ratio), and U (offshore longshore current speed) were examined in numerical experiments on synthetic embayments. Embayment bathymetry was found to have little impact on gyre characteristics. For a particular aspect ratio and offshore current velocity, the TKE and circulation within the embayment increase with decreasing corner angle. The variability of the circulation magnitude is significant for corner angles between $\alpha = 40°$ and 55°, whereas gyres do not form when α is greater than 60°. Narrower embayments result in more efficient transformation of the offshore velocity momentum to the TKE and circulation within the embayment. These results are consistent with previous findings on the separated shear layer in open cavity flows with incoming turbulent flows [5, 8, 18]. In particular, eddies within the embayment were found to be strongly dependent on the leading edge configuration and embayment Ar. For lacustrine embayments, the momentum gradient at the upstream edge is the most critical factor causing vertical vorticity vectors in the shear layer between embayment flows and the offshore current. The 2D turbulent flow advects these vertical structures into the embayment. Further inside the embayment, vortices with equal sign merge and give rise to recirculation current patterns.

The synthetic numerical results were shown to predict the behavior of embayment circulation in Lake Geneva. For this lake, where flows are mainly wind-driven, changes in the wind direction

lead to variations in the large-scale gyre configuration in the Grand Lac (Fig. 1) [33], causing changes in the longshore current direction in the vicinity of Vidy Bay and Morges Bay. These changes, although small, may alter circulation patterns, as can be seen in the case of Vidy Bay, where the angle between the alongshore current and the leading edge of the embayment is close to the critical angle of $\alpha = 60°$. Compared to Vidy Bay, the corresponding angle for Morges Bay is greater, and therefore gyre formation is more likely to take place in Morges Bay than in Vidy Bay. The probability of gyre formation in Morges Bay is further enhanced by an aspect ratio that is slightly narrower than that of Vidy Bay.

Acknowledgments

The research reported here was carried out with the support of the Swiss National Science Foundation (PDAMP2-123017 and P2ELP2-158885).

References

1. Rueda FJ, MacIntyre S (2010) Modelling the fate and transport of negatively buoyant storm–river water in small multi-basin lakes. Environ. Model Softw. 25: 146-157, doi:10.1016/j.envsoft.2009.07.002.

2. Venayagamoorthy SK, Ku H, Fringer OB, Chiu A, Naylor RL, Koseff JR (2011) Numerical modeling of aquaculture dissolved waste transport in a coastal embayment. Environ Fluid Mech. 11: 329-352. doi:10.1007/s10652-011-9209-0.

3. Albert DA, Wilcox DA, Ingram JW, Thompson TA (2005) Hydrogeomorphic classification for Great Lakes coastal wetlands. J Great Lakes Res. 31: 129-146, doi:10.1016/S0380-1330(05)70294-X.

4. Chang K, Constantinescu G, Park S (2006) Analysis of the flow and mass transfer processes for the incompressible flow past an open cavity with a laminar and a fully turbulent incoming boundary layer. J Fluid Mech. 561: 113-145, doi:10.1017/S0022112006000735.

5. Shankar PN, Deshpande MD (2000) Fluid mechanics in the driven cavity. Ann Rev Fluid Mech. 32: 93-136, doi:10.1146/annurev.fluid.32.1.93.

6. McCoy A, Constantinescu G, Weber L (2008) Numerical investigation of flow hydrodynamics in a channel with a series of groynes. J Hydraul Eng. 134: 157-172, doi:10.1061/ASCE0733-94292008134:2157.

7. Erturk E (2009) Discussions on driven cavity flow. Int J Num Meth Fluids. 60: 275-294, doi:10.1.1.342.5055.

8. Jackson TR, Haggerty R, Apte SV, Coleman A, Drost KJ (2012) Defining and measuring the mean residence time of lateral surface transient storage zones in small streams. Water Resour Res. 48: W10501, doi:10.1029/2012WR012096.

9. Langendoen EJ, Kranenburg C (1993) Simulation of unsteady flow in harbors. Adv Hydrosci Eng. 1: 1612-1617, doi:10.3923/jas.2011.962.970.

10. Uijttewaal WSJ, Booij R (2000) Effects of shallowness on the development of free-surface mixing layers. Phys Fluid. 12: 392-402, doi:10.1063/1.870317.

11. Shen J, Wang HV (2007) Determining the age of water and long-term transport timescale of the Chesapeake Bay. Estuar Coast Shelf Sci. 74: 585-598, doi:10.1016/j.ecss.2007.05.017.

12. Signell RP, Beardsley RC, Graber HC, Capotondi A (1990) Effect of wave-current interaction on wind-driven circulation in narrow, shallow embayments. J Geophys Res. 95: 9671-9678, doi:10.1029/JC095iC06p09671.

13. Elwell FC (2004) Flushing of Embayments. Unpublished PhD thesis, Queens' College, University of Cambridge, UK. http://www.damtp.cam.ac.uk/lab/people/fcg21/thesis.pdf. last accessed on 4 November 2016.

14. Apel JR (1987) Principles of Ocean Physics. Academic Press, New York, USA.

15. Razmi AM, Barry DA, Bakhtyar R, Le Dantec N, Dastgheib A, Lemmin U, Wüest A (2013) Current variability in a wide and open lacustrine embayment in Lake Geneva (Switzerland). J Great Lakes Res. 39: 455-465, doi:10.1016/j.jglr.2013.06.011.

16. Grace SM, Dewar WG, Wroblewski DE (2004) Experimental investigation of the flow characteristics within a shallow wall cavity for both laminar and turbulent upstream boundary layers. Exp Fluids. 36: 791-804, doi:10.1007/s00348-003-0761-3.

17. Rockwell D, Naudascher E (1978) Review–Self-sustaining oscillations of flow past cavities. J Fluids Eng. 100: 152-165, doi:10.1115/1.3448624.

18. Booij R (1989) Depth averaged k-ε-model in ODYSSEE. Tech Rep 1-89, Section of Hydraulic Engineering, Faculty of Civil Engineering, Delft University of Technology, Delft, The Netherlands.

19. Dimotakis P (1986) Two-dimensional shear-layer entrainment. AIAA J., 24: 1791-1796, doi:10.2514/3.9525.

20. Grace SM, Dewar WG, Wroblewski DE (2004) Experimental investigation of the flow characteristics within a shallow wall cavity for both laminar and turbulent upstream boundary layers. Exp Fluids. 36: 791-804, doi:10.1007/s00348-003-0761-3.

21. Caton F, Britter R, Dalziel S (2003) Dispersion mechanisms in a street canyon. Atmos Environ. 37: 693-702, doi:10.1016/S1352-2310(02)00830-0.

22. Corcos GM, Sherman FS (1984) The mixing layer: Deterministic models of a turbulent flow. Part 1. Introduction and the two-dimensional flow. J Fluid Mech. 139: 29 - 65, doi:10.1017/S0022112084000252.

23. Delft3D, http://www.deltaressystems.com/hydro/product/621497/delft3d-suite, last accessed on 4 November 2016.

24. D-Flow, http://www.deltaressystems.com/hydro/product/621497/delft3d-suitehttps://oss.deltares.nl/web/delft3d/d-flow-flexible-mesh. last accessed on 4 November 2016.

25. Van Delden A (1992) The dynamics of meso-scale atmospheric circulations. Phys. Rep. 211, 251–374.

26. Razmi AM, Barry DA, Lemmin U, Bonvin F, Kohn T, Bakhtyar R (2014) Direct effects of dominant winds on residence and travel times in a wide and open lacustrine embayment: Vidy Bay (Lake Geneva, Switzerland). Aquat Sci 76 (Suppl 1): S59-S71, doi:10.1007/s00027-013-0321-8.

27. Swiss Federal Office of Topography (2008) Formulas and constants for the calculation of the Swiss conformal cylindrical projection and for the transformation between coordinate systems.

https://www.swisstopo.admin.ch/content/swisstopo-internet/en/online/calculation-services/_jcr_content/contentPar/tabs/items/documents_publicatio/tabPar/downloadlist/downloadItems/20_1467104436749.download/refsyse.pdf. last accessed on 4 November 2016.

28. Margot J, Kienle C, Magnet A, Weil M, Rossi L, de Alencastro LF, Abegglen C, Thonney D, Chèvre N, Schärer M, Barry DA (2013) Treatment of micropollutants in municipal wastewater:

Ozone or powdered activated carbon? Sci Total Environ. 7: 480-498, doi:10.1016/j.scitotenv.2013.05.034.

29. Ashcroft G, Zhang X (2005) Vortical structures over rectangular cavities at low speed. Phys Fluids. 17: 015104, doi:10.1063/1.1833412.

30. Rockwell D, Knisely C (1979) The organized nature of flow impingement upon a corner. J Fluid Mech. 93: 413-432, doi:10.1017/S0022112079002573.

31. Shen C, Floryan J (1985) Low Reynolds number flow over cavities. Phys Fluid. 28: 3191-3202, doi:10.1063/1.865366.

32. Rockwell D, Naudascher E (1978) Review–Self-sustaining oscillations of flow past cavities. J Fluids Eng. 100: 152-165, doi:10.1115/1.3448624.

33. Lemmin U, D'Adamo N (1996) Summertime winds and direct cyclonic circulation: Observations from Lake Geneva. Ann Geophysicae. 14: 1207-1220, doi:10.1007/s00585-996-1207-z.

414 **Table 1.** Summary of the numerical experiments. Figure 2 shows the definition of the geometry.

Ar	Offshore velocity U (cm s $^{-1}$)	Corner angle α (°)	*L* (km)	Depth (m)
2	0.1, 1, 5, 10	0, 20,40	2	40
3	5	0, 20, 40, 50	3	40
4	0.1, 1, 5, 10	0, 20, 40, 50, 55, 60	4	40
6	5	0, 20, 40, 50, 55, 60	6	40
8	5	0, 20, 40, 50, 55, 60	8	40
4	5	50	4	80
4	5	50	4	10

415

Table 2. Wind characteristics, observed at Pully meteorological station (Fig. 1).

Starting date of the wind event	Wind regime	Wind duration (h)	Averaged wind velocity (m s^{-1})	Averaged wind angle* (°)	Type of measurement
8 Aug 2011	Bise	11	1.4	27	Drifter
15 Jan 2012	Bise	16	2.6	17	ADCP
3 Feb 2012	Bise	48	3.6	40	ADCP

* Wind angles in this study are based on azimuth and the "coming from" direction

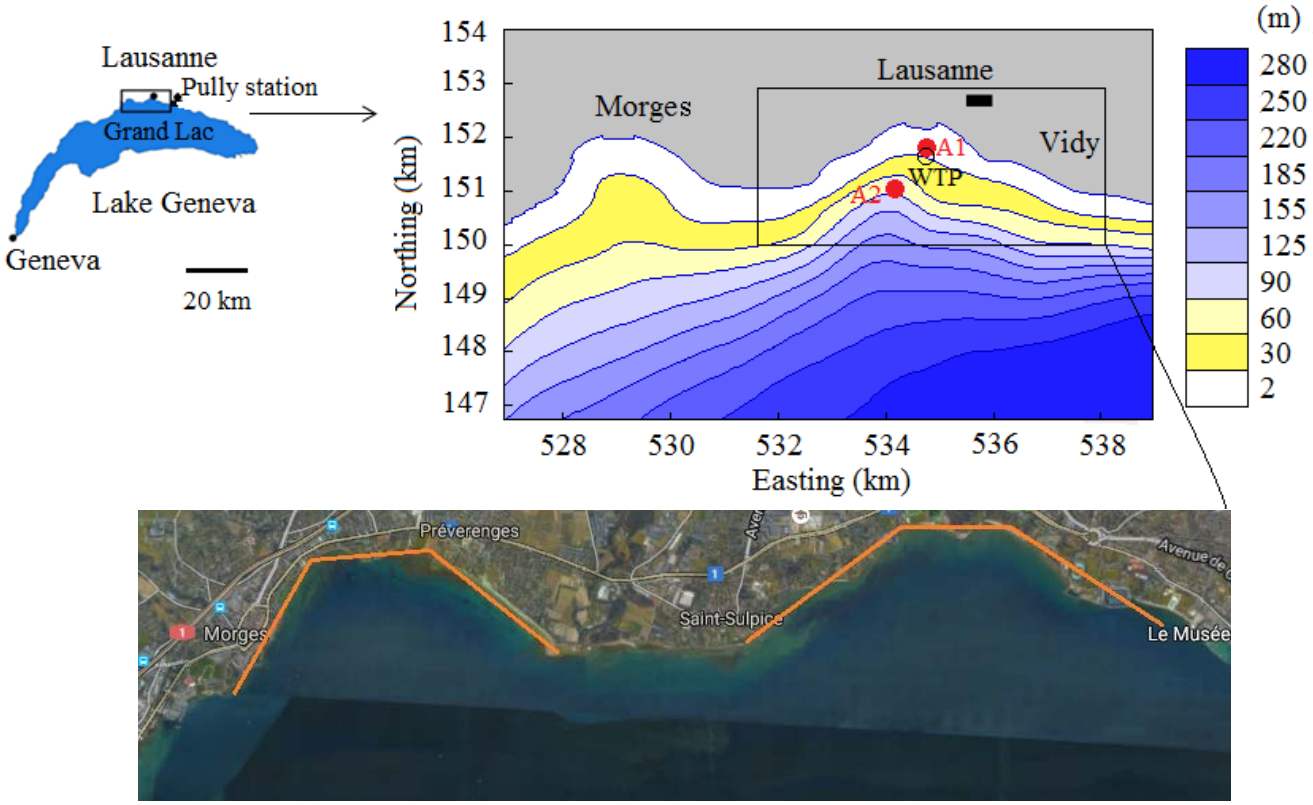

Figure 1. Location of Vidy Bay and Morges Bay in Lake Geneva. The Pully meteorological station, ADCP measurement locations (A1 and A2) and the WTP outfall are indicated. The color bar shows the lake depth contours. The image (Google Earth) with the inferred geometries (orange lines) of Vidy Bay and Morges are also shown.

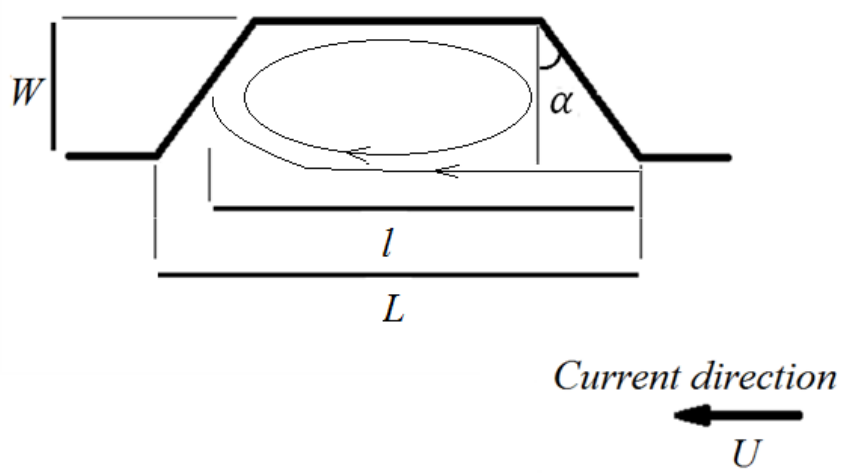

Figure 2. Embayment geometry used in the numerical analysis. The embayment is defined by its width (*W*), length (*L*) and corner angle (α). The offshore velocity is *U* and the reattachment distance from the leading edge is *l*.

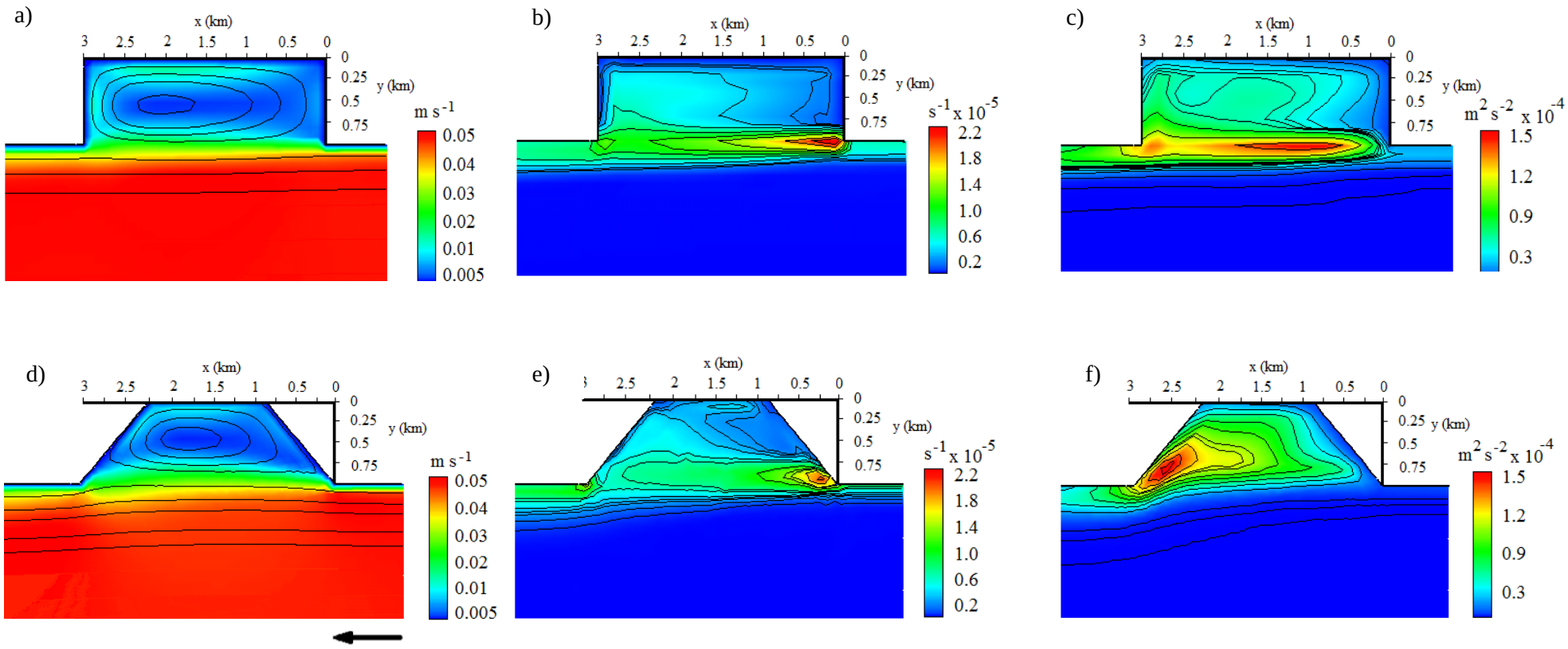

Figure 3. 2D view of simulated depth-averaged velocity magnitude with streamlines (left column), vorticity contours (center column) and TKE (right column) for two synthetic embayments: U = 5 cm s^{-1}, Ar = 3, corner angles of α = 0° (a-c), α = 40° (d-f). The current is parallel to shore in both cases, as shown by the solid vector beneath plot (d). The plots are based on quasi-steady state model resul

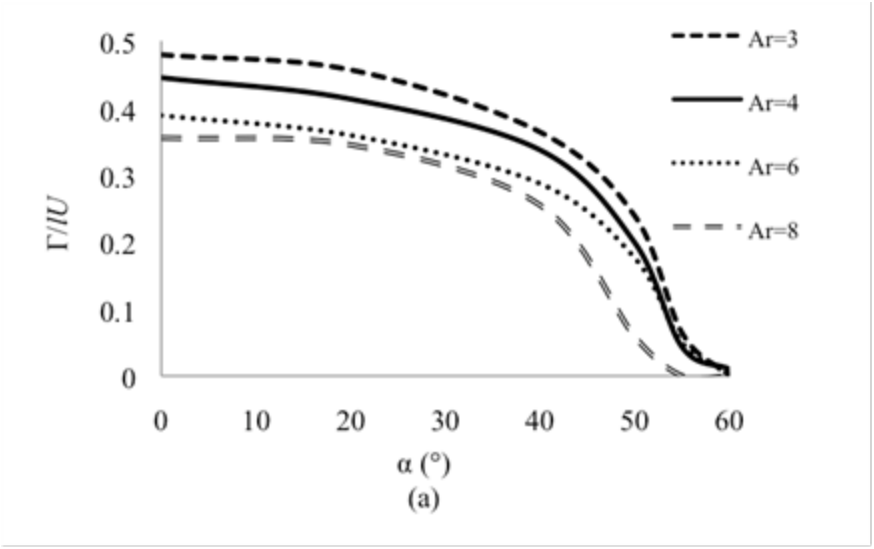

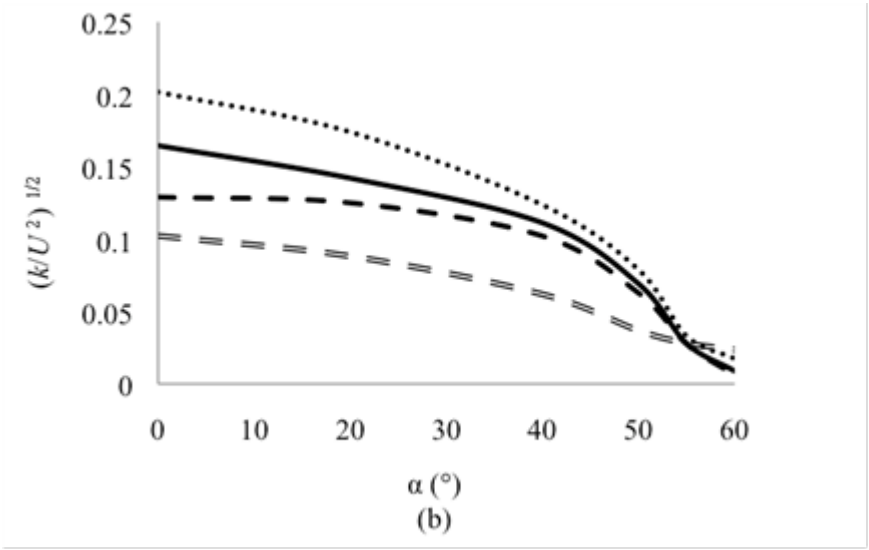

Figure 4. (a) Normalized circulation versus corner angle, α, and (b) normalized TKE, *k*, versus α. *U* = 5 cm s-1 for all cases. Circulation starts around α = 55° and increases with decreasing embayment corner angle.

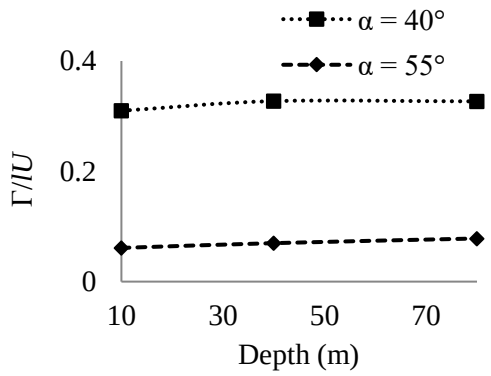

436

437 **Figure 5.** Variation of normalized circulation with depth for *Ar* = 4, and corner angles of α =
438 40 and 55° for $U = 5$ cm s^{-1}.

439

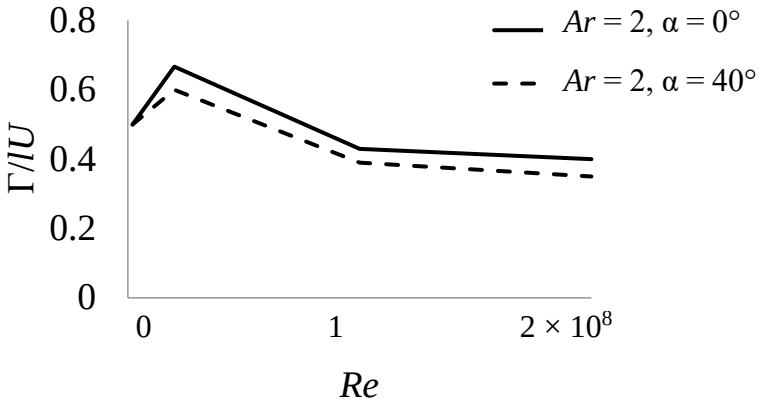

(a)

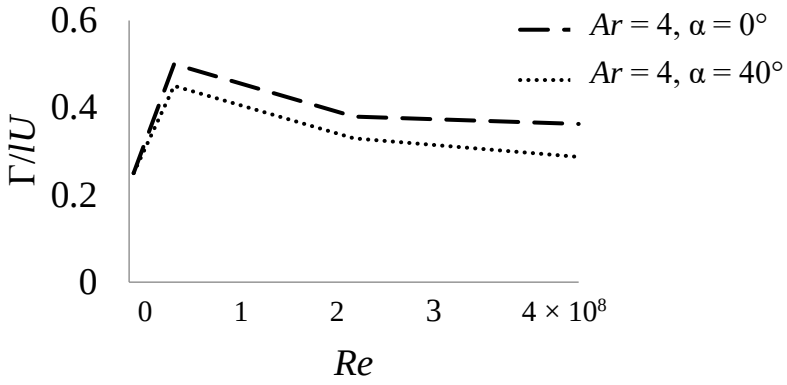

(b)

Figure 6. Variation of non-dimensional circulation (Γ/lU) with *Re* for $\alpha = 0$ and 40° at (a) *Ar* = 2 and (b) *Ar* = 4.

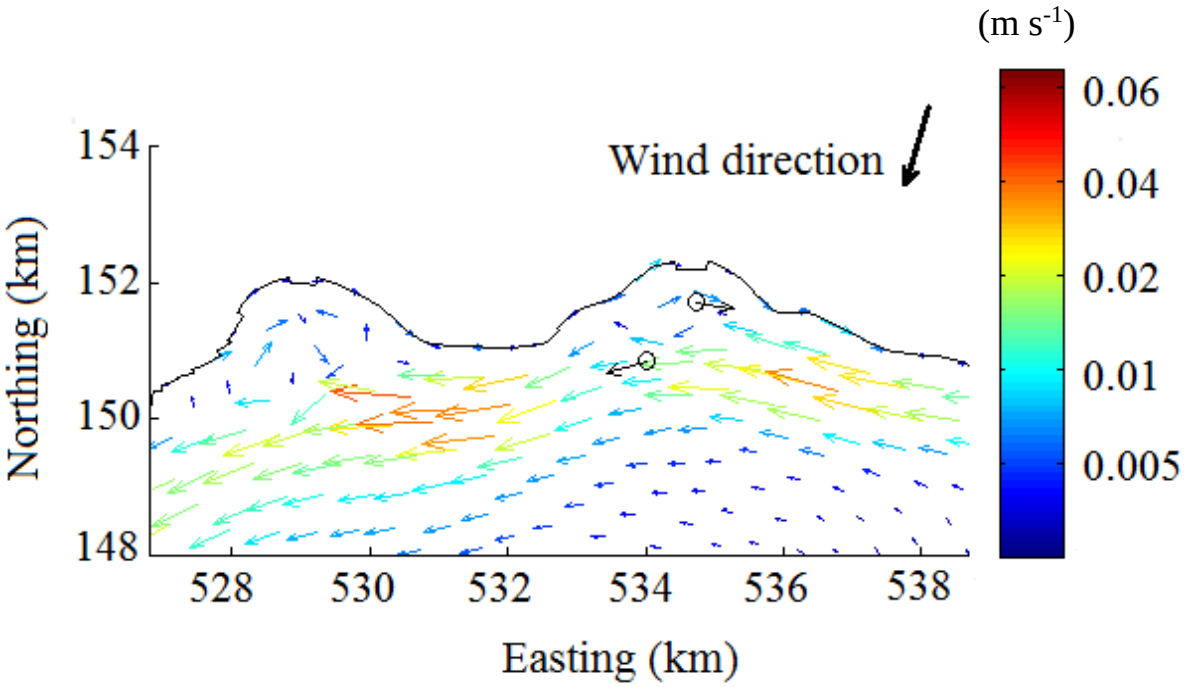

(a)

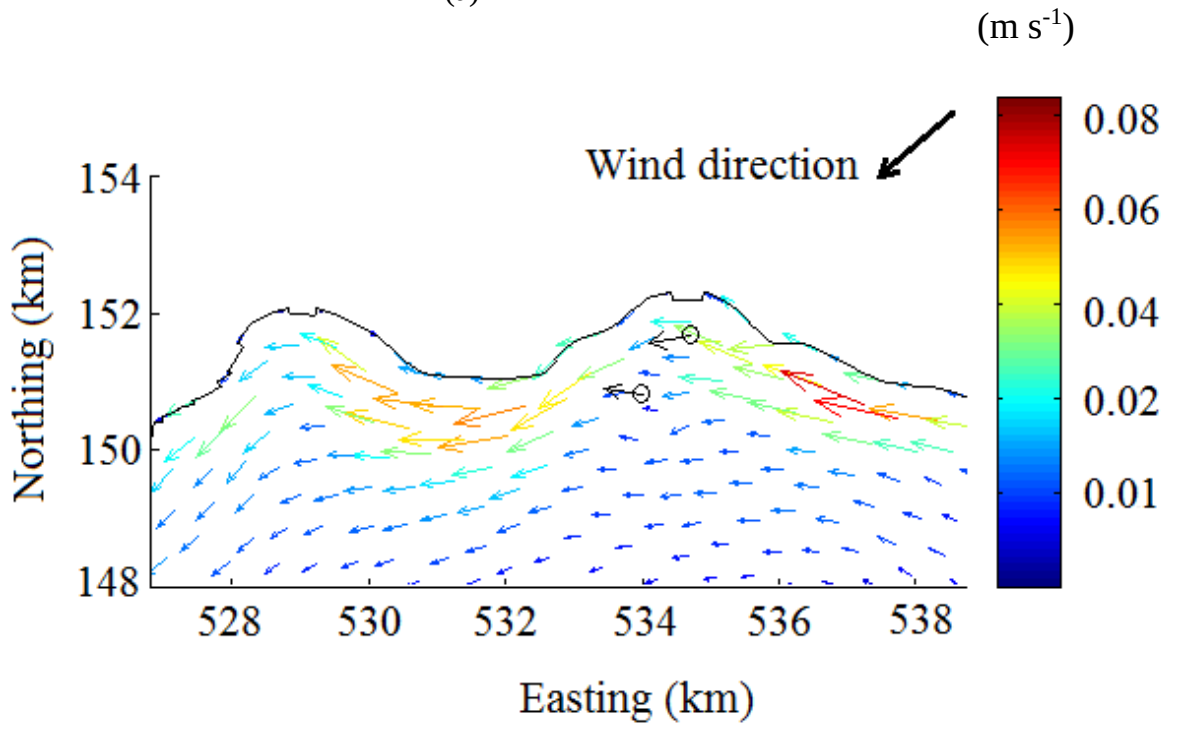

(b)

Figure 7. Computed depth-averaged velocity vector maps accompanied by measured velocity vectors in Vidy Bay under Bise wind events. The vectors averaged over the wind event (Table 1) (a) 15-16 Jan 2012 (gyre formation) and (b) 3-5 Feb 2012 (no gyre). Circles show the location of the ADCPs and black vectors are depth-averaged measured velocity vectors. The color bar shows the current velocity magnitude.

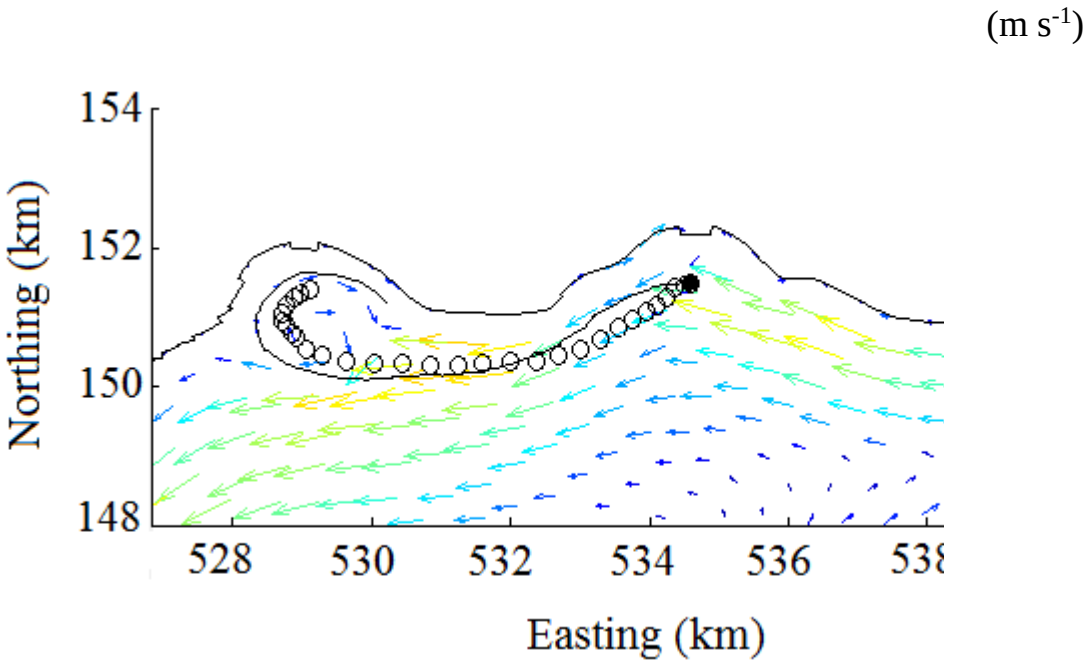

Figure 8. Near-surface velocity vector maps overlaid with computed and measured drifter patterns in Vidy Bay and Morges Bay on 9 Aug 2011. Circles are the measured drifter tracks and the solid line is the corresponding path computed from Delft3D-FLOW. The color bar shows the current velocity. The starting location of the drifter release is shown by the black circle.